In situ quantification of ultra-low O2 concentrations in oxygen minimum zones

Application of novel optodes

Larsen, Morten; Lehner, Philipp; Borisov, Sergey M.; Klimant, Ingo; Fischer, Jan P.; Stewart, Frank J.; Canfield, Donald Eugene; Glud, Ronnie N.

Published in:
Limnology and Oceanography: Methods

DOI:
10.1002/lom3.10126

Publication date:
2016

Document version
Final published version

Document license
CC BY

Citation for pulished version (APA):
Larsen, M., Lehner, P., Borisov, S. M., Klimant, I., Fischer, J. P., Stewart, F. J., Canfield, D. E., & Glud, R. N. (2016). In situ quantification of ultra-low O_2 concentrations in oxygen minimum zones: Application of novel optodes. *Limnology and Oceanography: Methods*, *14*(12), 784-800. https://doi.org/10.1002/lom3.10126

LIMNOLOGY
and
OCEANOGRAPHY: METHODS

ASLO

Limnol. Oceanogr.: Methods 14, 2016, 784–800

doi: 10.1002/lom3.10126

In situ quantification of ultra-low O_2 concentrations in oxygen minimum zones: Application of novel optodes

Morten Larsen,*[1] Philipp Lehner,[2] Sergey M. Borisov,[2] Ingo Klimant,[2] Jan P. Fischer,[3] Frank J. Stewart,[4] Donald E. Canfield,[1] Ronnie N. Glud[1,5,6,7]

[1]Institute of biology, Nordic Center for Earth Evolution (NordCEE), University of Southern Denmark, Campusvej 55, Odense, Denmark
[2]Institute of Analytical Chemistry and Food Chemistry, Graz University of Technology, Stremayrgasse 9, Graz, Austria
[3]Pyro Science GmbH, Hubertusstr. 35, Aachen, Germany
[4]School of Biology, Georgia Institute of Technology, Ford Environmental Sciences & Technology Building, 311 Ferst Drive, Atlanta, Georgia
[5]Scottish Association for Marine Science, Scottish Marine Institute, Oban, Scotland, UK
[6]Greenland Climate Research Centre (CO Greenland Institute of Natural Resources), Kivioq 2, Box 570, Nuuk, Greenland
[7]Arctic Research Centre, Aarhus University, Aarhus, Denmark

Abstract

Conventional sensors for the quantification of O_2 availability in aquatic environments typically have limits of detection (LOD) of >1 μmol L^{-1} and do not have sufficient resolution to reliably measure concentrations in strongly O_2 depleted environments. We present a novel trace optical sensor based on the palladium(II)-benzoporphyrin luminophore, immobilized in a perfluorinated matrix with high O_2 permeability. The trace sensor has a detection limit of $\sim$5 nmol L^{-1} with a dynamic range extending up to $\sim$2 μmol L^{-1}. The sensor demonstrates a response time <30 s and a small, predictable, and fully reversible response to hydrostatic pressure and temperature. The sensor showed excellent stability for continuously measurements during depth profiling in Oxygen Minimum Zones (OMZ). The novel sensor was deployed in situ using a Trace Oxygen Profiler instrument (TOP) equipped with two additional O_2 optical sensors, with higher dynamic range, allowing, when combined, measurements of O_2 concentration from $\sim$5 nmol L^{-1} to 1000 μmol L^{-1} with a single instrument. The TOP instrument was deployed in the OMZ regions of the Eastern Tropical North Pacific (ETNP) and Bay of Bengal (BoB). The measurements demonstrated that O_2 concentrations in the ETNP generally were below the LOD of the trace sensor, but that large sub-micromolar O_2 intrusions, spanning 60–80 m with maximum O_2 concentrations above 50 nmol L^{-1}, could be observed in the OMZ core. The O_2 concentrations in the BoB were high compared to the ETNP and rarely decreased below 50 nmol L^{-1}, but demonstrated tremendous small-scale variability.

The methods and sensors typically used to quantify O_2 concentrations in aquatic environments are based on standard Winkler titrations (Grasshoff 1983; Winkler 1888), electrochemical methods (e.g., Revsbech 1989; Martini et al. 2007), and only more recently, the use of optical sensors (Tengberg et al. 2006; Chipman et al. 2012; Kirf et al. 2014*b*). The majority of these techniques, however, have LOD's of >1 μmol L^{-1}. While such measurements are adequate for many investigations, they do not have sufficient resolution to reliably measure O_2 concentrations in strongly O_2 depleted environments, such as marine oxygen minimum zones (OMZ's) where O_2 concentrations can fall below 10 nmol L^{-1} (Revsbech et al. 2009; Thamdrup et al. 2012; Tiano et al. 2014; Ganesh et al. 2015).

To date, in situ submicromole O_2 concentrations in OMZ's have only reliably been measured using electrochemical STOX sensors (Switchable Trace OXygen) (Revsbech et al. 2009, 2011). The high sensitivity of the STOX sensor is achieved by a switchable front guard. The front guard electrochemical removes all O_2 at the tip of the sensor, thus allowing in situ calibration of the zero signals, minimizing uncertainties caused by, for example, fluctuating temperature, electronic drift, and zero offsets. For typical STOX

Additional Supporting Information may be found in the online version of this article.

*Correspondence: mortenl@biology.sdu.dk

sensor measurements, the front guard is switched on/off in a cyclic pattern, with a period of 30–75 s (Revsbech et al. 2011), representing the time to obtain a single measurement point. With STOX sensors it is generally possible to detect and quantify O_2 concentrations of ~10 nmol L^{-1} (Revsbech et al. 2009, 2011). With this high sensitivity, STOX sensors have substantially improved our understanding of O_2 dynamics and concentrations within OMZ regions (Kalvelage et al. 2011; Dalsgaard et al. 2012; Thamdrup et al. 2012; Ulloa et al. 2012; Tiano et al. 2014; Ganesh et al. 2015). However, the production and use of these sensors require highly specialized expertise and very few laboratories mastered their production (Revsbech et al. 2011). Furthermore, the commercially available STOX sensors are costly. These constraints have limited our advancement in resolving and understanding how the availability and dynamics of O_2 regulate key biogeochemical processes in OMZ's (Ulloa et al. 2012) and other low-oxygen environments.

O_2 optodes offer an attractive alternative to STOX methodology for trace O_2 sensing. O_2 optodes with high sensitivity (LOD ~1–50 nmol L^{-1}) are relatively easy to manufacture, and they typically feature a nonlinear response that significantly enhances the resolution and the signal to noise ratio at low O_2 concentrations (Lehner et al. 2015). While trace O_2 optodes have been applied to laboratory-based measurements (Nestler et al. 2007; Holtappels et al. 2014; Ganesh et al. 2015; Lehner et al. 2015), in situ-based systems have not had sufficient sensitivity for measurements in OMZ regions. Furthermore, such sensors have not been adequately tested for the influence of changing hydrostatic pressure on signal response, limiting their application for in situ deployments. To our knowledge, in situ trace optical sensors (LOD ~10 nmol L^{-1}) have so far only been applied in relatively shallow limnic environments (Kirf et al. 2014a,b).

The sensing material in optodes is traditionally a two-component system, composed of an indicator and a polymer matrix. While several luminescent O_2 indicators exist, only a few are frequently used for monitoring O_2 in aquatic environments (Quaranta et al. 2012). The function of the matrix is to physically entrap the indicator, to eliminate undesired cross-talk from ionic species and to offer the possibility of tuning the sensitivity of the sensors by using matrices with different permeabilities (Draxler et al. 1995; Koren et al. 2013). For all O_2 optodes, the dynamic range spans about three orders of magnitude. Accordingly, the dynamic range of a "standard" optical O_2 sensor is typically ~0.5–1000 μmol L^{-1}, whereas available trace sensors with a LOD of ~ 50 nmol L^{-1} typically have a dynamic range up to ~60 μmol L^{-1}. Therefore, given the low upper range of highly sensitive optodes, it is necessary to use a combination multiple sensor to span the O_2 gradient typical of OMZ regions, where O_2 can range from >200 μmol L^{-1} to <10 nmol L^{-1} in the OMZ core.

Here, we present and evaluate a novel trace O_2 sensor design that combines a long-lived palladium(II)-fluorinated benzoporphyrin luminophore, immobilized in a highly O_2-permeable perfluorinated polymer, allowing detection and quantifications of ultra-low O_2 concentrations of down to ~5 nmol L^{-1}. The optical trace range sensor has been deployed together with mid-range and standard range O_2 optodes, integrated in a stand-alone trace oxygen profiler (TOP) instrument. The TOP instrument was used to resolve O_2 availability and dynamics within the OMZ of the Eastern Tropical North Pacific (ETNP) and the Bay of Bengal (BoB). The optode results are compared and discussed in relation to pressure and temperature effects and with respect to concurrent measurements with STOX sensors.

Easily manufactured optical sensors allow detailed in situ measurements of O_2 concentration in a range from ~5 nmol L^{-1} to 500 μmol L^{-1} by a single instrument—an ability that will markedly advance our present understanding of biogeochemical processing in OMZ's and other highly O_2-depleted aquatic environments.

Materials and procedures

Optical sensors principle and design

Luminescent-based optical sensors are based on the ability of O_2 to act as a dynamic quencher, reducing the luminescent intensity and the lifetime of the O_2 indicator (Kautsky 1939; Klimant et al. 1995), allowing quantification of the O_2 partial pressure. Two of the most commonly used indicator classes are ruthenium(II) polypyridyl complexes and platinum(II) porphyrins (Quaranta et al. 2012), the latter being increasingly popular due to higher brightness and longer luminescent lifetime. Platinum(II) porphyrin indicators have been more broadly applied during the last decade (Tengberg et al. 2006; Borisov et al. 2008; Larsen et al. 2011), allowing the design of sensors with higher O_2 sensitivity.

We designed three sensors (standard-, mid- and trace-range) that in combination allow measurements of O_2 concentration from ~1000 μmol L^{-1} to ~5 nmol L^{-1} by using a combination of two different luminescent O_2 indicators and two different polymers. The standard-range sensor is based on a platinum(II) tetra(4-fluorophenyl)tetrabenzoporpyhrin indicator (Pt-TPTBPF) (Borisov et al. 2011) immobilized in polystyrene (PS). The mid-range sensor is based on a palladium(II) tetra(4-fluorophenyl)tetrabenzoporpyhrin (Pd-TPTBPF) (Borisov et al. 2008) immobilized into PS. Finally, the trace-range sensor is based on the same palladium(II)-tetrabenzoporpyhrin indicator as used for the mid-range, modified to allow immobilization in Teflon® AF1600 (AF). Hereafter, we refer to the standard-, mid- and trace-range as Pt-PS, Pd-PS, and Pd-AF, respectively (Table 1).

The Pt(II) indicators typically have a luminescent lifetime ~40–70 μs in the absence of O_2 (Oguri et al. 2006; Wang and Wolfbeis 2014). In comparison, the Pd(II) indicators have a much longer lifetime (~350–1000 μs) under the same conditions (Quaranta et al. 2012; Wang and Wolfbeis 2014). The significantly longer lifetime of the Pd(II) indicators

Table 1. Typical performance of the three sensors types. $d\tau 0/dT$; % decrease in $\tau 0$ for 1 °C temperature increase. dK_{SV}/dT; % increase in K_{SV} at 1 °C temperature increase. $d\tau 0/dB$ % decrease in $\tau 0$ at a 100 bar increase in hydrostatic pressure. dK_{SV}/dB change in K_{SV} at 100 bar increase in hydrostatic pressure. For the Pt-PS and Pd-PS sensors, the dK_{SV}/dB value, represents the values obtained assuming a linear trend – see text for explanation. ‡Defined at 20°C, 0 bar, salinity 0. Values in brackets represent ± Standard deviation (n = 3-6).

	Upper dynamic range [μmol L^{-1}] †	LOD [nmol L^{-1}]†	K_{SV} [(μmol L^{-1}) $^{-1}$]†	$d\tau 0/dT$ (%°C^{-1})	K_{SV}/dT (%°C^{-1})	$d\tau 0/dB$ (% pr. 100 Bar)†	dK_{SV}/dB (% pr 100 Bar)†	Response time (t_{90}) (s) †
Pt-PS Standard-range	~1000	~200	0.017	−0.078 (0.35 × 10^{-2})	0.964 (0.035)	−0.238 (1.27 × 10^{-3})	−3.21 (0.62)	<5
Pd-PS Mid-range	~50	~50	0.167	−0.255 (0.38 × 10^{-2})	0.894 (0.024)	−0.219 (2.0 × 10^{-3})	−3.21 (0.62)	<20
Pd-AF Trace-range	~2	~5	2.18	−0.166 (0.69 × 10^{-2})	0.618 (0.023)	−0.952 (4.8 × 10^{-2})	2.18 (0.070)	<30

makes them ideally suited for highly sensitive O_2 sensors. This is especially true when the Pd(II) indicators are immobilized into highly gas-permeable matrices such as AF, where the O_2 permeability is ~136 times higher than that of PS (Arcella et al. 2003; Bikson et al. 2004). An additional benefit of AF is that it has a very high chemical stability. This stability prevents chemical reaction of photosensitized singlet O_2 with the polymer backbone resulting in consumption of O_2 and therefore inaccurate results (Koren et al. 2013).

Compared to the commonly used Pt(II) and Pd(II) porphyrins (Lee and Okura 1997; Amao and Okura 2009), the indicators used in this study rely on tetrabenzoporphyrins. The tetrabenzoporpyhrin indicators feature a strong absorption in the region from nm 600 to 630 nm and an emission in the near infrared (NIR) range (Borisov et al. 2008). The red excitation light and NIR emission have the advantages of low interference with ambient background light and autofluorescence from the excitation light.

The tetrabenzoporphyrin indicators used in this study are directly compatible with the commercially available FiresStingO2-mini optical oxygen meters (Pyro science, GmbH). The FireSting excites the indicators with a 620 nm LED and measures the luminescent lifetime of the indicators using the phase modulation method (Holst et al. 1995; Schmälzlin et al. 2005) eliminating the interference by ambient light.

Sensing chemistry and sensor construction

feedthrough construction

The indicator dyes were synthesized as described in Borisov et al. (2008, 2009). The Pt- and Pd-TPTBPF indicators show good solubility in PS. However, in order to ensure compatibility of the O_2 indicator with the perfluorinated AF matrix and to avoid dye aggregation, the palladium(II)-benzoporpyhrin was modified with one perfluorooctyl chain via radical perfluoroalkylation, according to (Li et al. 2010), using perfluorooctyl iodide as a reagent and copper as a catalyst in dimethylsulfoxide. Analogously, the Pt(II) complex with one perfluorooctyl chain immobilized in AF was used for investigation of pressure effects (see later).

For all types of sensors, 1% (wt/wt) of the indicator with respect to the polymer was used. For the standard and mid-range sensors, the cocktail was a 10% (wt/wt) PS solution in chloroform. For the trace sensors a 5% (wt/wt) solution of AF in octafluorotoluene was used. The sensing "cocktail" was coated onto the tip of an Ø1 mm glass fiber by dipping the tip of the fiber in the sensing cocktail. The tip of the glass fiber had been rounded with a high-temperature flame. Prior to dip coating, the fibers for the PS-based sensors were treated with trimethylchlorosilane, and the AF based sensors were treated with fluoroalkylmethylchlorosilane (Aquaphobe® CF, Gelest) to ensure good adhesion of the polymers to the glass fiber. The ~50 mm long fibers were inserted into

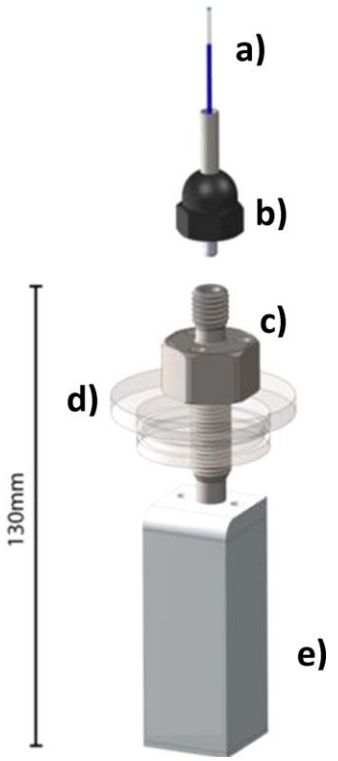

Fig. 1. Drawing of the sensor assembly, optical feedthrough, and oxygen meter. (a) Ø 1 mm glass fiber with "sensing chemistry" attached to the tip of the fiber. The blue section is a protective polymer coating. The glass rod is inserted into a simplex fiber optic connector. A dome nut (b) is used to press the optical connector to the optical feedthrough (c). On the drawing the feedthrough is mounted through the lid of a small pressure vessel (d). The opposite end of the feedthrough is directly attached to the optical oxygen meter (e) on the low pressure side.

a simplex fiber optic connector (Avago Technologies, HFBR-4501Z) and fixed with cyanoacrylate adhesive.

The sensor assembly was mated with a specially designed and now commercially available optical feedthrough (Subport, PyroScience, GmbH) (Fig. 1). The feedthrough is based on an Ø3 mm sapphire glass rod acting as a direct coupling between the fiber and the FireSting oxygen meter on the low-pressure side. The feedthrough has a UNF 7/16-20 thread and can penetrate bulkheads up to 30 mm. The feedthrough is designed to withstand a hydrostatic pressure of 600 bar. The sensor assembly is pressed against the sapphire glass rod using a stainless steel dome nut with a 1.5 mm hole at the center (Fig. 1). The end of the feedthrough is inserted into the oxygen meter and fixed using a set screw.

Sensor calibration

Sensor calibration was performed using a digital gas mixer (SensorSense BV) by mixing N_2 (99.999%) with either atmospheric air or 0.1% O_2 in N_2. With the gas mixer and the available gasses, we could obtain O_2 concentrations between ~40 nmol L^{-1} and ~280 μmol L^{-1} with a minimum increase in O_2 of ~20 nmol L^{-1} (20°C, Salinity 0), based on the minimum increase in flow and the gasses used for the calibration The reported accuracy of the gas mixer output is ± 1% of given flow rate.

All gas lines were stainless steel or Vitron®. However, due to O_2 contamination in the source gases, it was not possible to reproducibly maintain O_2 levels below ~40 nmol L^{-1} within the gas mixer and gas lines. Absolute zero was defined from a solution containing 0.5% wt/vol sodium dithionite. Calibration was performed in a 0.5 L stainless steel cylinder filled with MilliQ water. The cylinder was sealed with a stainless steel lid, fitted with the optical feedthrough. The outflow from the gas mixer flushed the water in the cylinder via a G18 stainless steel needle inserted into the cylinder through an Ø2 mm hole in the lid. Typically, a calibration curve was generated from 6 to 10 points across the dynamic range of the respective sensors. Generation of a single calibration curve typically took 3–4 h, independent of the sensor type. Calibration was generally repeated three times.

All calibrations were performed at a fixed temperature by placing the cylinder in a thermostat-controlled cooling bath (VWR MX07R-20). During the calibration, the temperature did not fluctuate by more than ± 0.2°C. Calibration curves were fitted using the modified Stern–Volmer equation (Klimant et al. 1995; Glud et al. 1996):

$$\frac{\tau}{\tau 0} = \alpha + \frac{1-\alpha}{1+K_{SV} \cdot p} \quad (1)$$

Where $\tau 0$ is the luminescent lifetime in the absence of O_2, τ is the luminescent lifetime in the presence of O_2 at a given partial pressure (p), K_{SV} is the Stern–Volmer quenching constant representing the sensitivity, and α is the nonquenchable fraction of the luminescent signal (Glud et al. 1996; Larsen et al. 2011). For in situ measurements, $\tau 0$ and K_{SV} were adjusted for changes in hydrostatic pressure and temperature as described in the following section.

To allow for two-point calibration during in situ measurements, we determined a fixed α value to each sensors type as derived from multipoint calibrations of the three different sensor types at different temperatures. For the Pt-PS, Pd-PS, and Pd-AF we derived a fixed α values of 0.10, 0.15, and 0.20, respectively. A total of 8–10 sensors of each type, were used to determine an appropriate α value.

For all sensor types, the two-point fit of Eq. 1 provided R^2 values above 0.999 (Fig. 2), when fitted to the multipoint calibrations and the differences in K_{SV} were typically no more than 1%, as compared to multipoint curve fitting with a fixed α value. The good fit across the temperature range also suggests that at the given conditions application of different α values would be negligible. We assume that α is unaffected by changes in hydrostatic pressure (see later).

Partial pressure was converted to concentrations using the solubility coefficients of (Garcia and Gordon 1992) and their corrected Eq. 8 at standard pressure (1013.25 mbar).

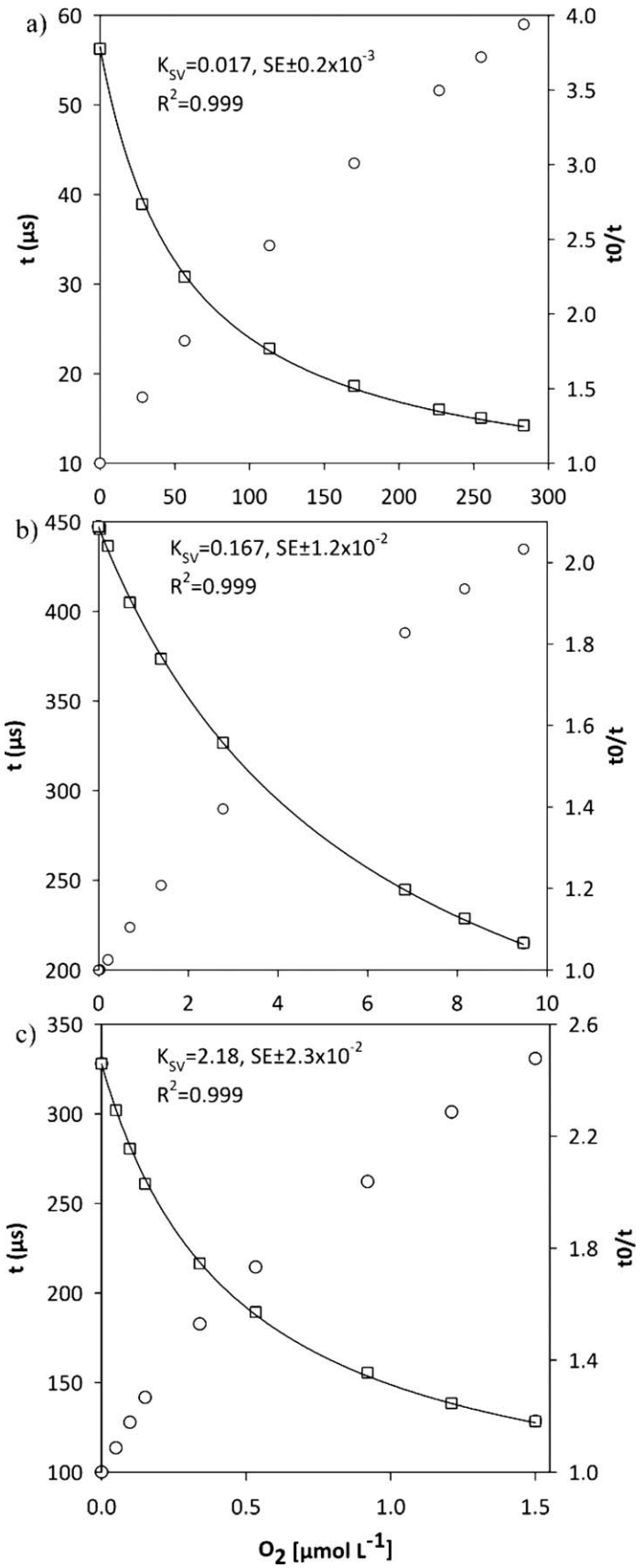

Sensor temperature and pressure compensation

In order to compensate for variations in temperature and hydrostatic pressure during in situ measurements, we determined the temperature and pressure effect on $\tau 0$ and K_{SV} for each of the three sensor types, applying the same calibration procedure as above. For each sensor type, we established calibration curves for three individual sensors using three to four different temperatures from 5°C to 20°C. The respective changes in K_{SV} and $\tau 0$ were calculated from the O_2 calibration curves obtained at these different temperatures.

The effect of hydrostatic pressure was investigated by pressurizing the water inside the calibration cylinder (Supporting Information Fig. S1). A pressure sensor with an analogue output (Sick, PBS 6041724) and a multi-fluid hand pump (Enerpac, MP-1000) was connected to the lid through a T-piece connection. From a reservoir connected to the hand pump, water was pumped into the cylinder, increasing the internal pressure in steps of ≥ 2 bar. The output from the pressure sensors was recorded with a 16-bit D/A converter (Measuring computing, USB-1608FS). Before the cylinder was pressurized it was filled with water via an overflow, assuring that no air was entrapped. During measurements, a glass coated rotating magnet ensured fully homogeneous conditions inside the pressure cylinder.

For each sensor type, three to six different sensors were tested in a pressure range from 1 to 400 bar. All pressure tests were performed at 20°C. The change in $\tau 0$ at increasing pressure was measured in sodium dithionite amended water (0.5% wt/vol).

As the change in K_{SV} at increasing pressure is primarily related to the properties of the matrix material (Glud et al. 1999), we carried out pressure tests for the PS and the AF matrix. For both matrices we used Pt(II) benzoporphyrin as the indicator. For both matrices we used the Pt(II) benzoporphyrin as the indicator. We chose to immobilize the perfluorooctyl modified version of Pt(II) benzoporphyrin into AF, enabling us to carry out the pressure investigations at O_2 levels higher that would otherwise have been possible with the Pd-AF. This was necessary as it proved impossible to reliably fill and maintain O_2 levels inside the cylinder below ~2% air saturation, due to O_2 contamination/ingress from the pressure pump.

For the Pt-PS sensors the pressure response was also evaluated at 15 different O_2 levels, ranging from ~5% to 100% air

Fig. 2. Multipoint calibration curves (τ) and Stern-Volmer plots ($\tau 0/\tau$) for the Pt-PS (a), Pd-PS (b), and Pd-AF (c) at 20°C. From the response of the different sensors, it can be observed how the sensitivity increases at decreasing O_2 levels and how the dynamic range of the sensors is reduced as the sensitivity is increased. For all sensors, the response can be fitted with a two-point fit, using the modified Stern–Volmer equation (Eq. 1) (solid line), with a fixed α-value of 0.10, 0.15, and 0.2, for the Pt-PS, Pd-PS, and Pd-AF sensor, respectively. Using a fixed α-value allows a two-point calibration to be performed. From the Stern–Volmer plots the nonlinear response can likewise be observed. Note the different scaling on the *x*-axis.

sat. For the Pt-AF sensor ten levels between 2% and 12% air saturation were used.

In situ instrumentation electronics

For in situ measurements, we designed a stand-alone instrument for TOP. The instrument contained four channels for optode measurements and two channels for STOX measurements. Data acquisition and hardware control was performed using a single board computer (SBC; fit-PC2i, CompuLab, 2MHz CPU, 2GB RAM), equipped with a 60 GB flash drive. The SBC was installed with a Windows 7© operating system, and controlled via a Windows© remote desktop through a SubConn® Ethernet bulkhead connector using a laptop or via a wireless connection. A remote desktop was used to operate all SBC programs and initiate data acquisition. Before deployment, the Ethernet communication cable was removed and the instrument operated fully autonomously. After profiling, the data acquisition was stopped and the recorded data were downloaded.

Data from four FireStingO2-Mini oxygen meters were recorded at 1 Hz using the PyroScience Oxygen logger software running on the SBC. The signals from two STOX electrodes were amplified by two custom-made picoamplifiers. The sensor front guard switching was controlled by a custom-made cyclic switch operating with a 60 or 30 s on/off cycle, depending on deployment. The signals from the STOX amplifiers and the front guard switching were recorded at 120 Hz using a 16-bit A/D converter (DT9816, Data Translation).

During initial configuration as used in the ETNP, pressure, and temperature were recorded by a Conductivity-Temperature-Depth profiler (CTD, Sea-Bird 911plus) deployed together with the TOP instrument. Subsequently, the timestamps of the instruments were aligned. In the ETNP the TOP instrument was mounted horizontally with the sensors pointing downwards. In the BoB, the instrument was mounted vertically underneath the CTD rosette. For both cruises, due to the placement of the instrument with the sensors closest to the bottom of the rosette, the down-cast CTD profiles had the best water exchange around the sensors. We, therefore, only present in situ depth profiles from the down-casts.

For deployments in the OMZ of the Bay of Bengal (see later) the instrument was upgraded with internally mounted pressure sensors (ECO ST1, Sensor Technik Sirnach AG) and temperature sensor (Pt-100, 4-wire, TS100, Sensor Technik Sirnach). The 4-wire signal from the TS100 sensor was recorded directly using one of the FireSting oxygen meters. The signal from the pressure sensor and two externally mounted sensors (conductivity (7-pole, AMT Analysenmesstechnik GmbH) and photosynthetically active radiation (PAR; QSP-2350, Biospherical instrument Inc.) was recorded using an A/D converter (DT9818, Data Translation) along with the signal from the two STOX sensors. The electronics were housed in a titanium cylinder (Ø; 180 mm, length; 760 mm) depth rated for 600 bar. The internal battery package (4 × 4500 mAh) ensured an operating time of > 12 h. The cylinder was fitted with a pressure relief valve to prevent potential pressure buildup inside the cylinder due to temperature increase (Dual O-Ring/SAE Port, DeepSea Power and Light).

In situ measurements

The TOP instrument was successfully deployed at eight stations in the ETNP as part of the Oxygen Minimum Zone Microbial Biogeochemistry Expedition (OMZoMBIE 1) cruise onboard the *R/V New Horizon* off the coast of Manzanillo, Mexico, in June 2013. Here, we present data from two stations: Sta. 2 (ETNP2; 18°55.218′N, 108°47.971′W); Sta. 6 (ETNP6; 18°55.145′N, 104°53.275′W). In addition, the upgraded instrument was deployed in January 2014 in the BoB at six stations during a cruise onboard *R/V Sagar Kanya* from Paradip to Chennai. Here, we present data from one station: Sta. 6 (BoB6, 15°99.666′N, 87°00.264′W).

The CTD data was sampled at 25 Hz, and subsequently down-sampled to 1 Hz. During the up-cast the CTD was positioned at discrete depths for 3–5 min to complete several STOX measuring cycles. The optical sensors were calibrated immediately before each deployment using a two-point calibration. The Pt-PS sensor was calibrated in a 0.5% (wt/wt) sodium dithionite solution and in 100% air saturated water. The Pd-PS and Pd-AF sensors were likewise zero calibrated in 0.5% (wt/wt) sodium dithionite. However, the second calibration point was obtained from the Pt-PS in situ measurements. The data from the Pt-PS, Pd-PS, and Pd-AF are presented with no smoothing of filtering. The maximum continuously deployment time for the sensors during the CTD casts were ~2 h.

During deployments in the ETNP and BoB the TOP-instrument was mounted on the CTD (Sea-Bird 911plus) equipped with a Sea-Bird Electronics 43 oxygen sensor (SBE43) and Seapoint or WETlabs chlorophyll fluorometer for the ETNP and BoB cruise, respectively.

Assessment

Sensor performance

Calibration of the three different sensors showed a K_{SV} of 0.017, 0.169, and 2.18 $(\mu mol\ L^{-1})^{-1}$ at 20°C for the Pt-PS, Pd-PS, and Pd-AF sensors, respectively (Table 1). These values demonstrate that the sensitivity of the Pd-AF sensor is approximately 100 and 10 times higher than for the Pt-PS and Pd-PS sensors, respectively. The upper limit for the dynamic range of the Pt-PS sensor is ~1000 $\mu mol\ L^{-1}$ at salinity 35°C and 20°C, which is comparable to most commercially available electrochemical and luminescence-based O_2 sensors for oceanographic research (Martini et al. 2007; Tengberg et al. 2006). The upper limits for the dynamic

ranges of the Pd-PS and Pd-AF sensors were ~50 μmol L^{-1} and 2 μmol L^{-1}, respectively (Table 1).

Due to the nonlinear response of the sensors (Fig. 2) the resolution is highest at low O_2 concentrations. Based on the noise of the $\tau 0$ (three times the standard deviation), the LOD for the sensors is estimated to be approximately 200 nmol L^{-1}, 50 nmol L^{-1}, and 5 nmol L^{-1} for the Pt-PS, Pd-PS, and Pd-AF sensors, respectively (Table 1).

The benzoporphyrin indicators used in this study demonstrate excellent photostability, brightness, and temporal stability (Borisov et al. 2008; Koren et al. 2013). The stability was demonstrated by continuous (1 Hz) measurements in a sodium dithionite solution for 24 h. The change in luminescent lifetime of the three sensors was less than 0.18×10^{-1}, 1.5×10^{-2}, and 7.1×10^{-2} ‰ h^{-1} for the Pt-PS, Pd-PS, and Pd-AF sensors, respectively; for all sensors this is below the respective LOD. The signal intensities change by 0.31×10^{-2}, 2.7×10^{-2}, 6.8×10^{-2} ‰ h^{-1}, respectively. The somewhat larger decrease in the signal for the intensity-based signal vs. the lifetime-based signal demonstrates the advantage of luminescent lifetime as compared to absolute intensity measurements. However, for both measurements, the stability was excellent.

The potential drift in K_{SV} for the Pd-AF sensors was investigated by repeating a multipoint calibration three times during 12 h at 15°C. Fitting the data points from the three calibration curves with a two-point calibration, the calculated mean K_{SV} was 2.124 (μmol L^{-1})$^{-1}$ SD $\pm$ 0.0102 and did not show any time-dependent drift. The K_{SV} calculate based on the multipoint calibration (with fixed α) did typically not deviate by more than 1%, as compared to the two-point calibration.

For measurements at 500 μmol L^{-1} with the Pd-AF sensors, an increase in the K_{SV} by 1% will induce an error of less than ~5 nmol L^{-1}. Thus, using a two-point calibration compared to a multipoint will not adversely affect the quality of the O_2 measurements. Calculating the O_2 concentration for each for the three curves using the mean K_{SV} demonstrated a good accuracy as compared with gas mixer output. The difference between the mean calculated O_2 concentration for the calibration curves and the gas mixer output was lower than ~12 nmol L^{-1} at concentrations below 1 μmol L^{-1}. The standard error of the mean for the three curves was generally below 10 nmol L^{-1}, with values > 5 nmol L^{-1} at concentrations below 500 nmol L^{-1}. The performance of the Pt-PS and Pd-PS sensors demonstrates the same degree of accuracy/precision and stability, thus all presented sensors can be used for typical CTD profiling with no need for drift correction. The response time for optical sensors depends on the thickness of the sensing layer as this controls O_2 diffusion into the sensing layer. Therefore, bright indicators allow for the construction of fast sensors, as even thin sensing layers have a sufficiently high luminescence for detection by the oxygen meter. The bright Pt-PS sensor enabled typical t_{90} response times of ~5 s, whereas the Pd-PS and Pd-AF had response times of approximately 20–30 s (Table 1). It should be noted that the response time represents the time for a 90% signal change and that the sensors will respond dynamically when profiling through an O_2 gradient. The response time of the Pd-PS and Pd-AF sensor can be increased by applying thinner sensing layers.

Effect of temperature and hydrostatic pressure on sensor response

The signal of all luminescent indicators is affected by changes in temperature due to thermal quenching (Quaranta et al. 2012) and correction of the sensor signal is essential for in situ measurements with changing temperature. For optical O_2 sensors calibrated by the modified Stern–Volmer equation (Eq. 1) the effect of temperature is accounted for by independent temperature correction of $\tau 0$ and K_{SV} (Rickelt et al. 2013).

For the three different sensors both $\tau 0$ and K_{SV} showed a linear temperature dependence ($R^2 > 0.99$) in the range of 5–20°C (Fig. 3; Table 1). The decrease in $\tau 0$ ranged between -0.078% C^{-1} and -0.255% C^{-1}, with the Pt-PS sensor demonstrating the lowest influence, followed by the Pd-AF and Pd-PS sensors, respectively. The decrease of $\tau 0$ with rising temperature is related to thermal quenching of the phosphorescence of indicators rather than to changes in physicochemical properties of the immobilization matrix (Borisov et al. 2011; Rickelt et al. 2013; Mcneil and D'asaro 2014). This is consistent with the fact that the two Pd(II)-porphyrin-based sensors had similar $\tau 0$ temperature coefficients that were approximately three times higher than the Pt(II)-dye based sensor (Table 1). The absolute values align with previously published values for temperature coefficients of these indicators (Borisov et al 2008). The temperature coefficient for K_{SV} ranged from 0.62%°C^{-1} to 0.96%°C^{-1} with the Pd-AF sensor demonstrating the lowest sensitivity, followed by the Pt-PS and Pd-PS sensors, respectively (Table 1). The increase in K_{SV} at increasing temperature is primarily due to the increasing permeability of the immobilization matrix. Therefore, the temperature coefficients of K_{SV} of the two PS-based sensors were similar (Table 1).

The effects of hydrostatic pressure on the performance of optical sensors have not been reported in great detail, and to our knowledge only a few studies have previously investigated pressure effects on O_2 optodes, with two lab investigations using optodes with PS as the matrix material (Glud et al. 1999; Tengberg et al. 2006) and two studies on the Aanderaa optodes response (Uchida et al. 2008; Mcneil and D'asaro 2014; Bittig et al. 2015). However, since hydrostatic pressure effects depend on both the mechanical, physical–chemical design of a sensor, O_2 solubility, and optical feedthrough, the hydrostatic effect needs to be evaluated for each specific design.

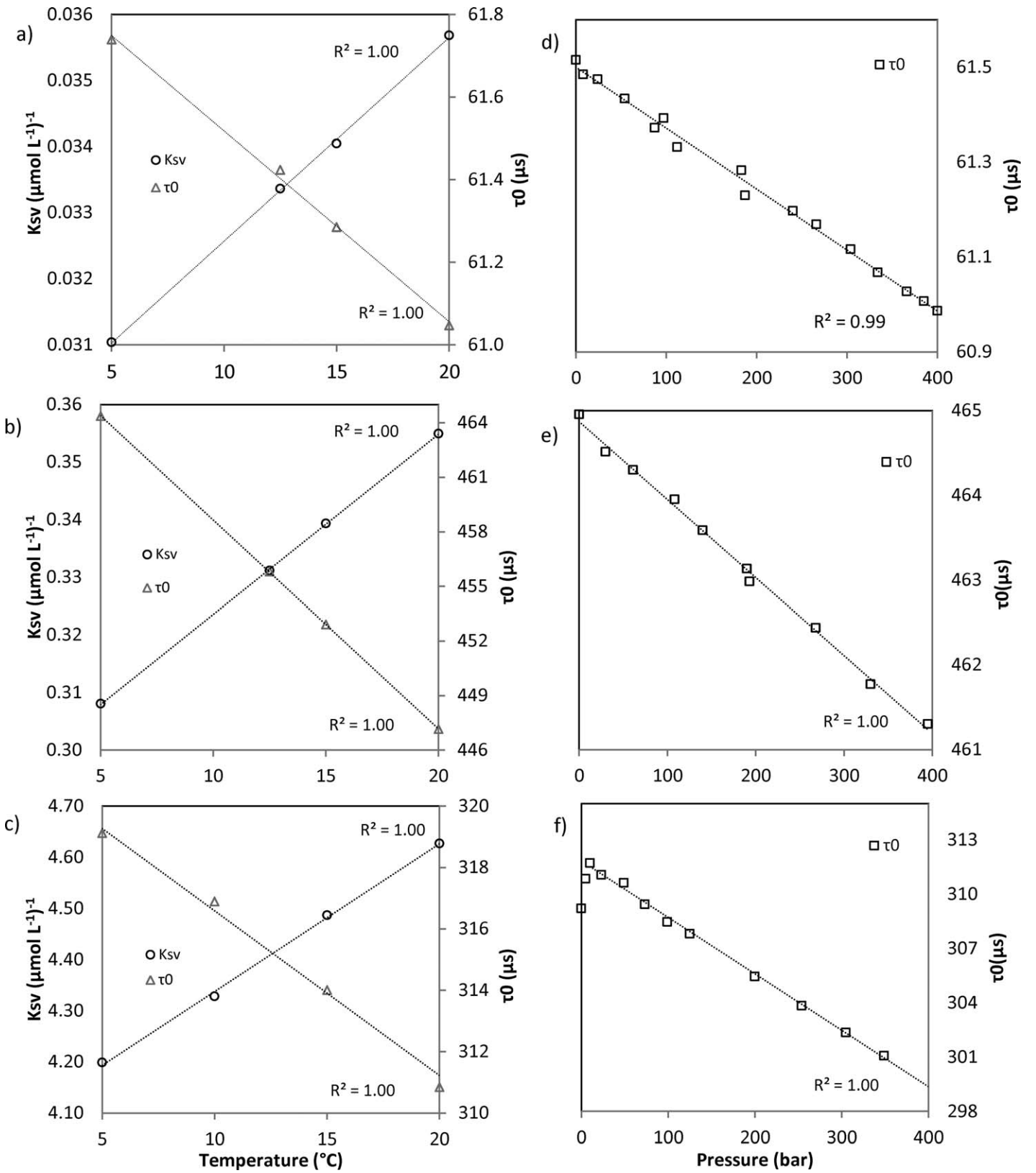

Fig. 3. Temperature effects on $\tau 0$ and K_{SV} for (a) Pt-PS (b) Pd-PS, and (c) Pd-AF at temperatures from 5 to 20°C from laboratory-based investigations. Both K_{SV} and $\tau 0$ for all sensors demonstrate a strong linear correlation with temperature (> 0.99). Hydrostatic pressure effect on $\tau 0$ for Pt-PS (d) Pd-PS (e), and Pd-AF (f) from 0 to 400 bar. The linear fit for the Pd-AF in panel (f) is from 10 to 350 bar.

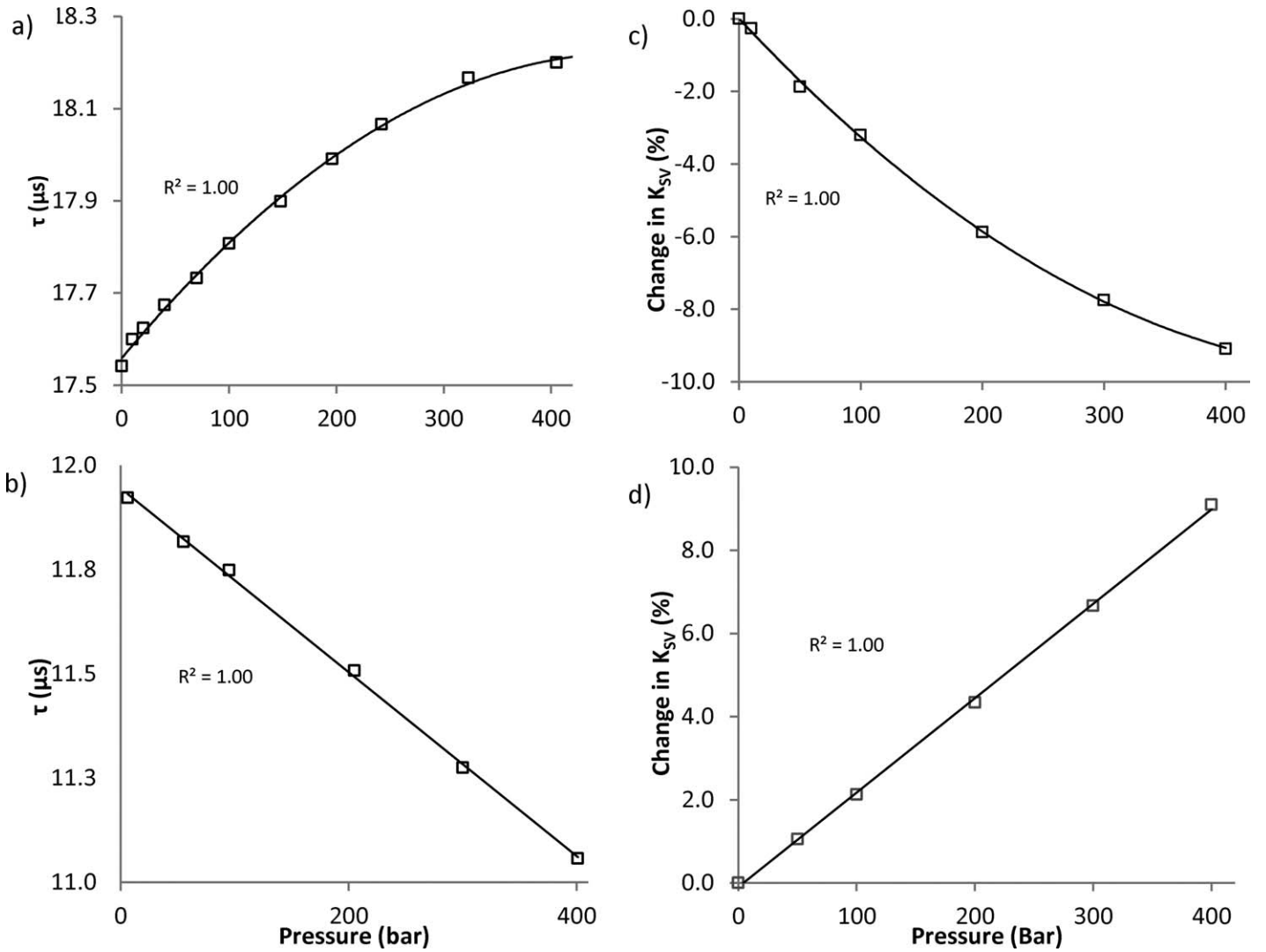

Fig. 4. Effect of hydrostatic pressure on τ and *K*SV for the PS and AF matrices with immobilized Pt(II) tetrabenzoporpyhrin. (a) and (b) example of changes in τ at ~70% air sat., and ~5% air sat., for PS matrix and AF matrix, respectively. (c) and (d) calculated effect of changes in hydrostatic pressure on K_{SV} for the PS matrix and AF matrix. The change in K_{SV} calculated for the PS matrix was applied to pressure compensates the Pt-PS and Pd-PS sensors and the effect on the AF matrix to compensate the Pd-AF sensor.

For all sensors we observed a decrease in $\tau 0$ with increasing pressure. Both PS-based sensors demonstrated a linear decrease in $\tau 0$ and signal intensity as a function of increasing pressure in the range from 0 to 400 bar (Fig. 3). The decrease in $\tau 0$ amounted to 0.22% and 0.24% pr. 100 bar increase, for the Pt-PS and Pd-PS sensor, respectively. For measurements near the sensors LOD an increase in pressure from 0 to 400 bar would equate to an apparent increase in O_2 concentration of ~0.7 μmol L^{-1} and ~0.1 μmol L^{-1} (5°C, salinity 35) for the Pt-PS and Pd-PS sensors, respectively.

The sensor based on AF did not show the same linear decrease in $\tau 0$ at increasing pressure. Instead, we consistently observed a small initial increase in $\tau 0$ and signal intensity as the pressure was increased to ~10 bar. However, this increase was subsequently followed by a pressure dependent linear decrease (Fig. 3f). The initial increase in $\tau 0$ corresponded to a ~1% increase and corresponds to an apparent underestimation in O_2 concentration of ~4 nmol L^{-1} (at 5°C, Salinity 35). The linear decrease in $\tau 0$ above ~10 bar corresponds to 0.95% pr. 100 bar (Fig. 3f), which is somewhat higher than for the PS-based sensors. For measurements near the sensors LOD an increase in pressure from 0 to 400 bar would correspond to an increase in apparent O_2 concentration of ~15 nmol L^{-1} at (5°C, Salinity 35). We found that the initial increase in $\tau 0$ of the Pd-AF sensor could be eliminated via coating the outer tip with an additional layer of AF containing TiO_2 (10% wt/wt). The additional coating with TiO_2 scattering layer significantly increases the signal intensity of the sensor as compared to the uncoated sensor. Increasing the signal intensity makes the sensor less affected by signal loss

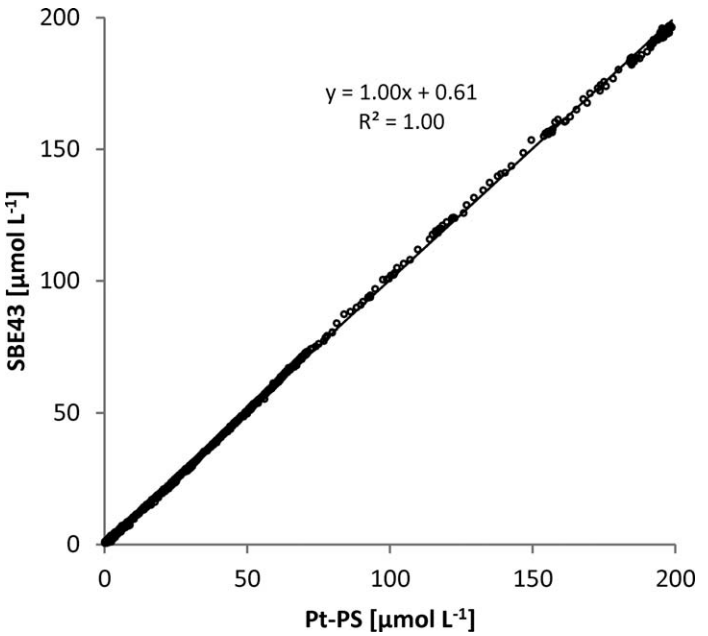

Fig. 5. Comparison of the measured in situ O_2 concentration from the SBE43 and Pt-PS sensor from BoB6. The measurement was performed during continuous down-cast profiling to a maximum depth of 1470 m. During the profiling the temperature decreased from 25.4°C to 4.3°C. The comparison shows an excellent agreement between the sensors, but also show a zero-offset of 0.61 μmol L^{-1} for the SBE43 sensor. It should be noted that the SBE43 offset could be largely eliminated if the sensor was recalibrated.

in the optical pathway due to the increased hydrostatic pressure.

As for temperature, the effect of hydrostatic pressure on K_{SV} is predominantly determined by the matrix polymer (Glud et al. 1999). We therefore only determined changes in K_{SV} for the PS and AF matrices using the Pt-TPTBPF and its perflurooctyl-modified version, respectively. For both matrices, the change in K_{SV} was determined based on the change in τ as function of pressure at ten to 15 different O_2 levels. For the PS matrix we observed a nonlinear increase in τ at increasing pressure. This trend was observed across the entire concentration range (Fig. 4a). Likewise, the K_{SV} also followed a nonlinear trend, with decreasing K_{SV} at increasing pressure (Fig. 4), corresponding to a decrease of approximately 3.21% pr. 100 bar increase, assuming a linear trend (Table 1).

For the AF matrix, τ decreased linearly with increasing pressure across the entire concentration range (Fig. 4b). Correspondingly, the K_{SV} increased linearly with increasing hydrostatic pressure, corresponding to a change of 2.18% pr. 100 bar (Table 1). The apparent change in O_2 concentration due to pressure effects on the K_{SV} value for the Pd-AF sensor at 50, 200, and 400 bar amounts to an overestimation of ~35 nmol L^{-1}, 200 nmol L^{-1}, and 400 nmol L^{-1} when exposed to 2 μmol L^{-1}. None of the sensors exhibited hysteresis during repeated pressure cycles or during compression vs. de-compression.

The effect of hydrostatic pressure on the sensor matrix is a complex interaction between several factors and a detailed evaluation of the respective components is outside the scope of this study. We note, however, the opposing pressure effects on K_{SV} for the PS and AF matrices, which underpin the need for careful evaluation of pressure effects on different sensor types prior to in situ application.

In summary, hydrostatic pressure had a small and reproducible influence on the sensor responses. However, similar to the temperature cross-talk, the predicable behavior allowed for effective pressure compensation and high precision measurements at changing hydrostatic pressure. Furthermore, the response at increasing hydrostatic pressure for the PS-based sensor agree with the previous findings of (Glud et al. 1999; Tengberg et al. 2006; Uchida et al. 2008; Mcneil and D'asaro 2014) for sensors with comparable sensitivity.

In situ OMZ measurements

The calibrated O_2 signals of the SBE43 and the Pt-PS sensors correlated extremely well in all deployments (Fig. 5). However, for all deployments the SBE43 was found to have a zero-offset ranging from ~0.61 μmol L^{-1} in BoB to ~2.2 μmol L^{-1} in the ETNP. Such zero-offset has previously been observed for commercially available oceanographic O_2 sensors, such as the SBE43 (Revsbech et al. 2009; Thamdrup et al. 2012; Ganesh et al. 2015).

The down-cast O_2 distribution at station ETNP2 as obtained with the SBE43 exhibited a steep decline in the O_2 concentration from the maximum concentration of ~220 μmol L^{-1} in the chlorophyll *a* (Chl *a*) maximum at ~55 m depth, reaching the zero-offset (~2.2 μmol L^{-1}) at ~160 m (Fig. 6a). Below 160 m, the concentration from the SBE43 remained relatively stable, increasing slightly with depth to reach 2.8 μmol L^{-1} at 800 m (Fig. 6a). At ~780 m a small increase in O_2 concentration of ~0.8 μmol L^{-1} above the zero-offset was observed. Apart from the small increase at 780 m, the O_2 profile from the SBE43 did not show a distinct structure and the mean O_2 concentration from 160 to 800 m, as resolved by the SBE43 sensor, was 2.25 μmol L^{-1} (SD ± 0.20 μmol L^{-1}).

In comparison, the concentration measured with the standard range Pt-PS sensor generally showed levels around the LOD (0.2 μmol L^{-1}) from ~230 to 660 m. But below 600 m the O_2 concentration gradually increased to a maximum of 0.59 μmol L^{-1} at 770 m. The Pt-PS data demonstrate that a well-calibrated luminescence-based sensor can provide improved O_2 resolution, compared to the standard O_2 sensor, such as the SBE43 sensor.

The Pd-AF trace sensor resolved significant spatial variation in sub-micromolar O_2 concentrations in the depth interval from 125 to 800 m (Fig. 6b). At 125 m, the concentration was 2.12 μmol L^{-1}, but dropped to ~25 nmol L^{-1} at 138 m, overlapping with the position of the secondary Chl *a*

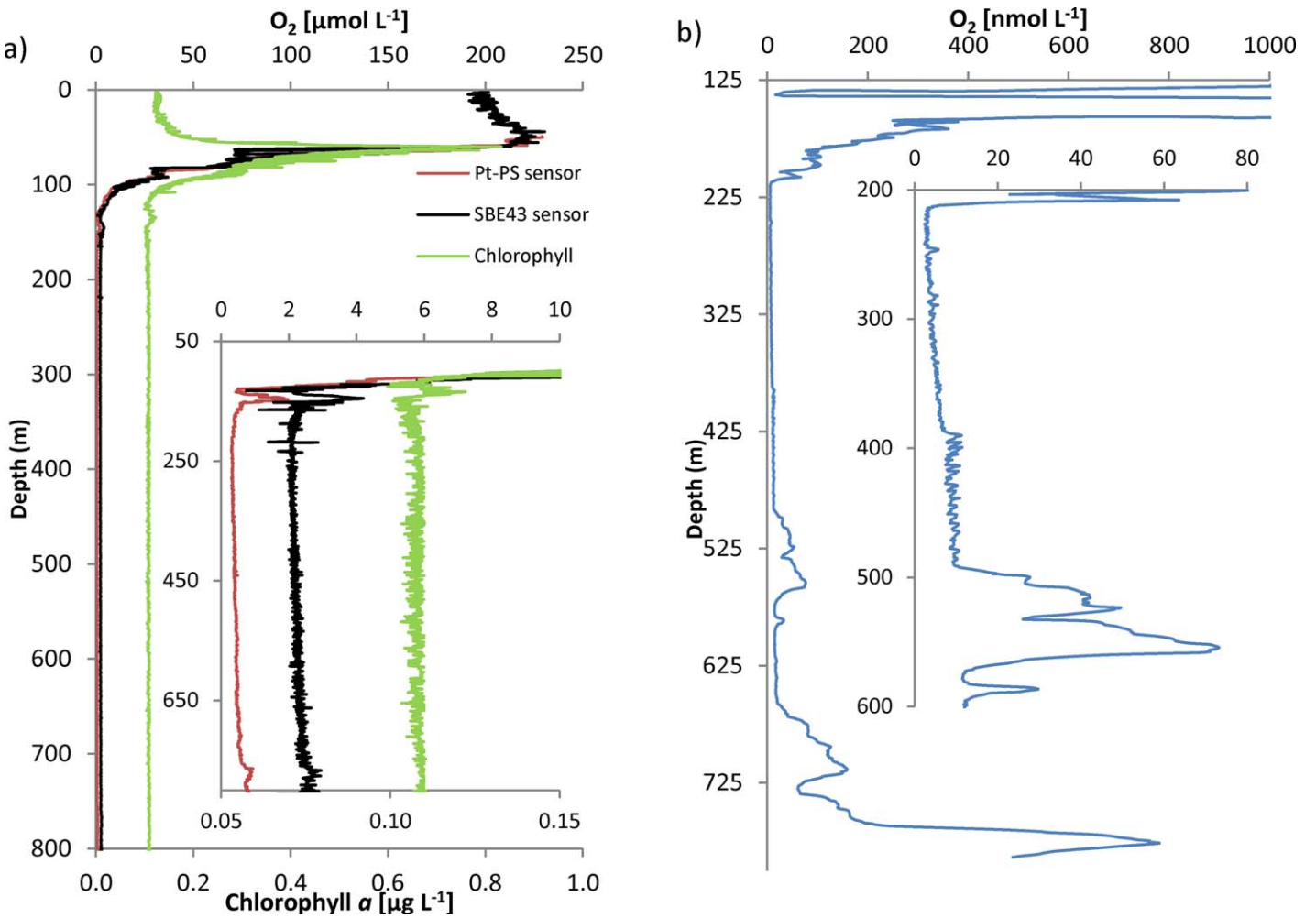

Fig. 6. Downcast in situ O_2 distribution from ETNP2. (a) The measured concentration from both the SBE43 sensor and the Pt-PS standard range sensors are shown together with chlorophyll *a* fluorescent measurements. Both O_2 sensor show an almost identical profile, however, as it can be observed on the small inset, the SBE43 sensor have a zero-offset of ~2.2 μmol L^{-1}, from ~140 m to 800 m. In the same depth interval, the mean O_2 concentration measured by the Pt-PS sensor is below zero-offset of the SBE43 sensors. At ~115 m to140 m a small secondary Chl *a* maximum can be observed, overlapping with an increase in the O_2, with a maximum concentration of ~2.1 μmol L^{-1}, as measured by the Pt-PS sensors. (b) In situ trace O_2 distribution measured with the Pd-AF sensor from the same CTD cast as presented in panel a, however, only measurements from 125 m to 800 m are shown and only concentrations below 1000 nmol L^{-1}. The inset shows a detailed view of the dynamics in the trace O_2 distribution at concentration below 80 nmol L^{-1} from 200 m to 600 m.

maximum (Fig. 6a). The concentration increased to 2.15 μmol L^{-1} at 146 m before gradually decreasing to concentrations below the LOD (5 nmol L^{-1}) of the sensor at 213 m. From 213 to 390 m, the measured concentration was generally below the sensor LOD. However, numerous microstructures with "spikes" of 2–3 nmol L^{-1} above the "background" concentration could be observed. At 390–490 m O_2 concentrations increased to 7–11 nmol L^{-1} and the frequency of the spikes became more regular. Below 490 m, larger O_2 intrusions could be observed. These intrusions spanned 60–80 m with maximum O_2 concentrations above 50 nmol L^{-1}. At 777 m O_2 concentration increased to 780 nmol L^{-1}. Looking closely at the Pt-PS profile in Fig. 6a, the contours of this rather large O_2 intrusion can be observed as an O_2 increase to 0.82 μmol L^{-1}, while this increase is barely visible in the SBE43 data. Two casts were performed at this station, both confirming the existence of the large sub-micromolar O_2 intrusions in the core of the OMZ.

Trace O_2 levels as resolved by optodes and STOX sensors

During the BoB cruise the TOP instrument was deployed with two Pd-PS and two STOX sensors. Generally, the O_2 concentration in the BoB rarely reached consistent stable concentrations below ~50 nmol L^{-1} (Bristow et al. unpubl.) and extensive O_2 dynamics at concentrations < 3 μmol L^{-1} could be observed (Fig. 7). The measured concentrations from the two Pd-PS sensors demonstrated an excellent

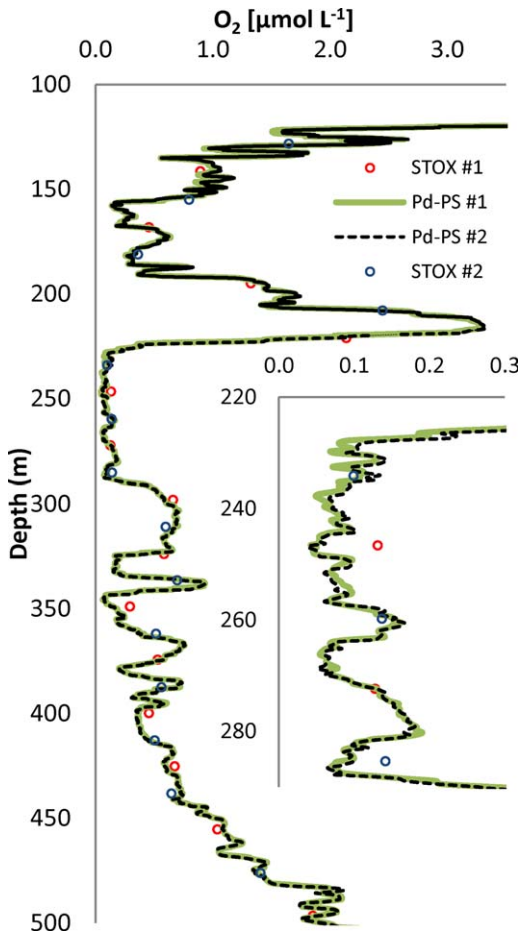

Fig. 7. In situ O_2 distribution from BoB6, measured with two Pd-PS sensors and two STOX sensors during continuously down-cast profiling. The STOX sensors were independently calibrated against the SBE43 sensor and operated out of phase to increase the temporal/spatial resolution. For the entire cast both Pd-PS sensors show excellent agreement and generally also a good agreement with the two STOX sensors. It can be observed on the inset that the O_2 concentration from 220 m to 300 m never consistently reach values below 50 nmol L^{-1}. Comparing the Pd-PS and STOX measurements, it can be observed that the relative slow measuring time of the STOX sensors is inadequate for quantifying the extensive small scale O_2 dynamics typically observed in BoB.

agreement with a mean difference between the two sensors below the sensors LOD. The dynamics and concentrations measured with the two optical sensors agreed well with the measurements from the two STOX sensors (Fig. 7). Generally, the agreement between concentrations measured by the STOX and Pd-PS sensors was better that 2%, in the range from the sensors LOD up to 20 μmol L^{-1}.

Discussion

It is apparent that standard range Pt-PS and SBE43 sensors do not have sufficient sensitivity for resolving O_2 concentrations and dynamics within the core of the OMZ as revealed by the highly sensitive Pd-AF sensor. Relying solely on the SBE43 data from the ETNP6, one could only infer that the O_2 concentration was below ~2 μmol L^{-1}, in the depth range from ~130 m to 800 m at Sta. 2, but otherwise uncertain of the true O_2 concentrations and of any small scale dynamics occurring.

However, measurements with the trace Pd-AF sensor demonstrate that water masses from approximately 225 m to 300 m had O_2 levels at the LOD of the sensor (~5 nmol L^{-1}) and that the remaining water column had O_2 concentrations in the core of the OMZ (~550 m) as high as 73 nmol L^{-1}, due to large-scale intrusions spanning 60–80 m. Closer inspection CTD data demonstrated that the O_2 intrusions in all cased coincided with increases in the sigma-theta value, suggesting that the OMZ core is composed of several water masses with different O_2 concentrations.

To obtain high precision in situ measurements it is important that sensor signals are effectively compensated for changes in temperature and hydrostatic pressure. As demonstrated by the lab-based temperature and pressure tests, for measurements in OMZ regions with typical pressure and temperature changes of ~100 bar and 20°C during CTD casts, the decrease in temperature would have the greatest effect on the sensor signal. However, such effects are highly predictable. Of the three sensors presented here, the Pd-PS (mid-range) sensor is most affected by changes in temperature (Table 1), as is clearly observed in the luminescent lifetime (τ) in situ data (Fig. 8).

During the deployment in the ETNP, both the temperature and pressure changed as the CTD was raised stepwise from 700 m to 350 m in waters with an O_2 concentration below the LOD of the Pd-PS sensor (~50 nmol L^{-1}). It can be observed that the measured in situ τ decreased ~4 μs from ~460 μs to 456 μs as the temperature increased by ~4°C and the pressure decreased by ~35 bar. Under the given pressure and temperature variations, a change in luminescent lifetime of ~4 μs would correspond to an apparent change in O_2 concentration of ~80 nmol L^{-1}. The change is, however, fully predictable, as observed by the $\tau 0(t,p)$ representing the calculated $\tau 0$ lifetime at the given in situ temperature and pressure. We assume that the influence of temperature on the hydrostatic pressure effect is insignificant, and therefore we only conducted pressure testing at one temperature. The excellent agreement between the measured and calculated τ, indeed suggests that potential temperature effects on the pressure compensation coefficients can be ignored under the given in situ conditions in the ETNP and BoB. A potential cross effect of temperature on the pressure compensation cannot be fully excluded and should, if relevant for the measurements, be further investigated.

The excellent agreement between the Pt-PS and SBE43 (Fig. 5) and the Pd-PS and STOX data (Fig. 7) also clearly validate the procedure for compensating sensor signals for pressure and temperature interference. That such compensation

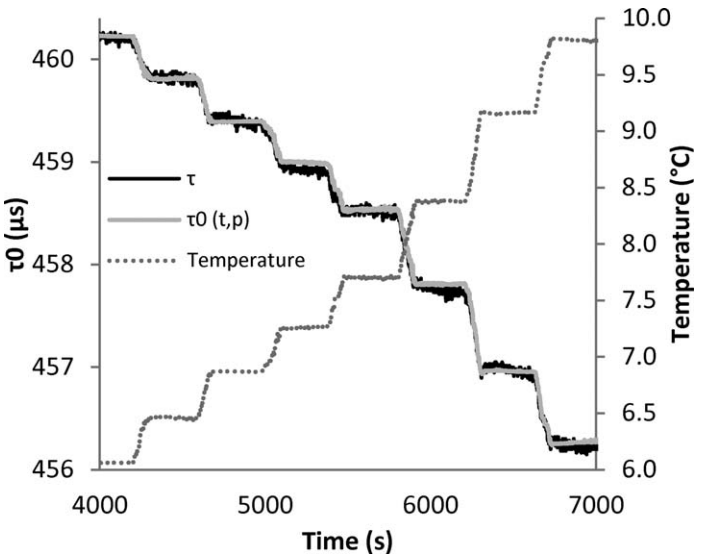

Fig. 8. Example of in situ temperature and pressure compensations of the luminescent lifetime from the Pd- PS sensor from ETNP6. The data were recorded during an up-cast where the O_2 concentration was below the LOD of the sensor. The CTD was stopped at ~5 min intervals at eight depths from 700 m to 350 m. τ represents the measured in situ luminescent lifetime of the sensor. $\tau 0(t,p)$ represents $\tau 0$, obtained from predeployment zero calibration, compensated for in situ temperature and pressure (p). From the measurements it is clearly observed how the luminescent lifetime of the Pd-PS sensor is affected by temperature (and to a less extent pressure), but this effect can effectively compensated for, as seen by the excellent agreement between the measured τ and the calculated $\tau 0(t,p)$.

is important is exemplified by the data in Fig. 5. If no compensation had been applied to the Pt-PS sensor signals, the sensor would have provided an O_2 concentration that underestimated the actual concentration by ~20 μmol L^{-1} at 1400 m depth.

The pressure and temperature compensation coefficients for different sensors of the same production batches generally demonstrated a good agreement, e.g., for six Pt-PS sensors from two different batches the mean change in $\tau 0$ was found to be -0.237 (SD $\pm 0.13 \times 10^{-2}$) and -0.235 (SD 0.96×10^{-2}), respectively. This suggests that the coefficients obtained for a single sensor can be applied to a batch of sensors and presumably the constants are universal for a given sensor type. This is further supported by the fact that in situ data obtained with the Pt-PS sensors in ETNP and BoB both showed an excellent agreement with the respective SBE43 sensor, even though the Pt-PS sensors for the two cruises were from different batches and the pressure/temperature compensation data were acquired from a third batch of sensors. However, we recommend that the temperature and hydrostatic responses of the different sensor types and batches are checked regularly to quantify batch variation and potential effects of polymer aging. Likewise, should the α value for each sensor type be assessed regularly, if the sensor are to be calibrated with a two-point calibration.

Correct calibration is essential for optimal sensor performance. As for the STOX sensors, the trace O_2 optode can be calibrated using a two-point calibration routine. One point can be recorded in sodium dithionate-amended water and the second point can be obtained from either deck calibration in a solution of known concentration or from in situ intercalibrations against other calibrated sensors (Revsbech et al. 2009). However, for such two-point calibrations the value of α must be determined from a multipoint calibration. As previously mentioned, the value of α can be determined for the specific sensor type and thus is in not necessary to determine α for individual sensors, as the α value is primarily related to the immobilization matrix.

Most available O_2 sensors (such as the SBE43), however, do not have the accuracy to allow direct in situ two-point calibrations of the trace sensors. In such cases, sensors with different dynamic ranges would have to be used, as was done here. Alternatively, the sensors can be calibrated using a ship-based two-point calibration. The two-point calibration should be performed with sodium dithionite and a premixed gas mix, e.g., 0.5% air saturation. Achieving the 0.5% air saturation with the compresses gas would require the use of a calibration vessel with minimized exposure to ambient air—such as shown on Supporting Information Fig. SI1—but otherwise the procedure would be identical to a calibration of a normal range sensor. Such calibration will in our opinion provide a reliable and relatively easy way to perform calibration of the trace sensor, provided that the data subsequently are correctly compensated for changes in temperature and pressure. We recommend that such two-point calibrations are performed as frequent as possible, ideally before each deployment. As noted previously, determination of the K_{SV} from a two-point calibration demonstrated that the K_{SV} did not typically deviate by more than 1%, when compared to the K_{SV} calculated from a calibration using eight or more points. For measurements at 500 μmol L^{-1} with the Pd-AF sensors an increase in the K_{SV} by 1% will induce an error of less than ~5 nmol L^{-1}. Thus, using a two-point calibration compared to a multipoint will not adversely affect the quality of the O_2 measurements.

However, pre-deployment ship-based multipoint calibration at fixed temperature is the preferred calibration approach. Such calibrations can ideally be performed with a gas mixer to obtain a multipoint calibration in the desired concentration range. A digital gas mixer similar to the one used in the presented study can be acquired for ~$5000.

The Teflon AF1600^{TM} matrix used for the trace sensors in this study represents an almost ideal polymer for high sensitivity sensors, due to its high O_2 permeability and good stability. However, to improve the stability of the trace sensors sensing "cocktail," we have investigated the use of the perfluorinated polymer Hyflon AD60 as an alternative to the trace sensor. The AD60 demonstrates better dye solubility and very low temperature dependence (Lehner et al. 2015).

However, with a permeability ~7 times lower than the AF1600 (Arcella et al. 2003), Hyflon AD60 has a somewhat higher LOD of ~10 nmol L^{-1}. Furthermore, initial pressure tests demonstrated that the AD60 matrix has very low dependence on hydrostatic pressure, lower than that of the AF and PS. The low temperature and pressure dependence of the matrix could potentially provide robust midrange O_2 sensors by immobilizing the Pt(II) porphyrin indicator in the AD60 matrix.

As for other aquatic sensors, biofouling could compromise sensor performance. This is especially true for trace in situ O_2 measurements, as O_2 consumption within any biofilm will significantly affect the measurements. To some extent the biofouling can be reduced by coating the sensing chemistry with a layer of antifouling material (Navarro-Villoslada et al. 2001) or by the direct addition of silver nanoparticles to the sensor matrix (Wencel et al. 2010), thereby significantly enhancing the operational lifetime of the sensor. In addition, sensors can be mechanically cleaned using a water jet (Tengberg et al. 2006) or through the application of sensor wipers (Delauney et al. 2010). However, for short term profiling in OMZ's, biofouling is not a major problem. Furthermore, biofilm formation on the perfluorinated materials (AF and Hyflon) is likely to be lower that for the standard polymers, such as PS.

With the TOP instrument and with the highly sensitive Pd-AF trace O_2 sensors, we have for the first time demonstrated the application of optodes for quantification of ultra-low O_2 concentrations, even at high hydrostatic pressure. With the trace O_2 sensors we have also for the first time documented high resolution measurements of sub-micromolar O_2 intrusions in the core of OMZ's. The extent and mechanism of such O_2 intrusion events in OMZs, however, remains to be explored. Doing so is critical, as variations in O_2 availability in the sub-micromolar range have been shown to have significant effects on rates of key microbial biochemical transformations (e.g., denitrification, anaerobic ammonium oxidation) in OMZs (Dalsgaard et al. 2012).

Our data demonstrate that improved insights into O_2 concentrations and dynamics in low-oxygen environments can be gained using trace O_2 sensors, as compared to traditional O_2 sensing technologies. Our observations in OMZs also highlight the need for additional trace sensor measurements to better understand the relationships between sub-micromolar O_2 dynamics in OMZ's and O_2-sensitive microbial processes.

Comments and recommendations

Compared to STOX sensors, the main advantages of the trace optodes is the simple production procedure combined with comparable or better response times and LOD. Calibration of the trace sensors is relatively simple and can be done using standard gas mixers or using pre-mixed gases. The described optodes show a predictable and reversible interference from temperature and hydrostatic pressure that can be effectively accounted for. One of the drawbacks of the optical sensors is the limited dynamic range of the specific sensors. Therefore, several sensors are required to fully cover the concentration range encountered in OMZ's. However, in most instances, commercially available O_2 sensors that are integrated in standard CTD instruments will adequately resolve O_2 concentrations down to ~1–2 μmol L^{-1}. We have, therefore, also developed a one-channel mini-TOP instrument that can be equipped with a single trace O_2 sensor that can be directly interfaced to a free analogue input channel of standard CTD's. Alternatively, measurements can be stored using the internal data logger on the mini-TOP. We envision that such mini-TOP instruments could be added to Argo floats, gliders or AUV's (Autonomous underwater vehicles) to provide sub-micromolar O_2 measurements in a wide range of O_2-depleted environments. However, for long-term deployments on e.g., Argo floats the sensors drift and stability needs to be better characterized.

In this study, we have used the Pt(II)- and Pd(II) tetrabenzoporphyrins indicators. However, these indicators can be substituted with the commercially available Pt(II) and Pd(II) complexes (5,10,15,20-tetrakis-(2,3,4,5,6-pentafluorphenyl)-porphyrin). Both indicators show good solubility in PS and Hyflon AD 60 matrices without further chemical modification (Lehner et al. 2015). One advantage of using the pentafluorophenyl-substituted porphyrins indicators is the longer luminescent lifetime when immobilized in the same polymers compared to the benzoporphyrins and hence an increased sensitivity. With such sensors and low noise readout devices (Lehner et al. 2015) a LOD of ~0.1 nmol L^{-1} become possible. However, even with low-cost color ratiometric methods (Stich et al. 2009; Larsen et al. 2011; Schutting et al. 2014; Santner et al. 2015), a LOD of ~0.5 nmol L^{-1} can be achieved. It should also be noted that optical feedthroughs for standard fiber optic cables rated for operation at full ocean depths are available from a range of manufacturers. Thus, multiple options exist for designing in situ sensors and instruments for trace O_2 sensing.

Laboratory experiments suggest that aerobic respiration can persist even at O_2 concentrations down to 3 nmol L^{-1} (Stolper et al. 2010). Thus, the LOD of 5 nmol L^{-1} of the trace sensors presented here may still be too high to fully document relevant O_2 dynamics in OMZ's. However, by using optical indicators with even longer luminescent lifetimes than Pd(II), such as boron- and aluminum chelates, sensors with LOD in the low pmol L^{-1} range could be realized (Lehner et al. 2014).

References

Amao, Y., and I. Okura. 2009. Optical oxygen sensor devices using metalloporphyrins. J. Porphyr. Phthalocyanines **13**: 1111–1122. doi:10.1142/S1088424609001455

Arcella, V., A. Ghielmi, and G. Tommasi. 2003. High performance perfluoropolymer films and membranes, p. 226–44 *In* N. N. Li, E. Drioli, W. S. W. Ho, and G. G. Lipscomb [eds.], Advanced membrane technology. Annals of the New York Academy of Sciences. New York Acad. Sciences.

Bikson, B., Y. Ding, J. K. Leroux, and J. K. Nelson. 2004. Gas separation using membranes formed from blends of perfluorinated polymers. Google Patents. http://www.google.com.na/patents/US6723152.

Bittig, H. C., B. Fiedler, P. Fietzek, and A. Körtzinger. 2015. Pressure response of Aanderaa and Sea-Bird oxygen optodes. J. Atmos. Oceanic Technol. **32**: 2305–2317. doi:10.1175/JTECH-D-15-0108.1

Borisov, S. M., G. Nuss, and I. Klimant. 2008. Red light-excitable oxygen sensing materials based on platinum(II) and palladium(II) benzoporphyrins. Anal. Chem. **80**: 9435–9442. doi:10.1021/ac801521v

Borisov, S. M., G. Nuss, W. Haas, R. Saf, M. Schmuck, and I. Klimant. 2009. New NIR-emitting complexes of platinum(II) and palladium(II) with fluorinated benzoporphyrins. J. Photochem. Photobiol. A **201**: 128–135. doi:10.1016/j.jphotochem.2008.10.003

Borisov, S. M., P. Lehner, and I. Klimant. 2011. Novel optical trace oxygen sensors based on platinum(II) and palladium(II) complexes with 5,10,15,20-meso-tetrakis-(2,3,4,5,6-pentafluorphenyl)-porphyrin covalently immobilized on silica-gel particles. Anal. Chim. Acta **690**: 108–115. doi:10.1016/j.aca.2011.01.057

Bristow, L. A., C. M. Callbeck, M. Larsen, M. A. Altabet, J. Dekaezemacker, M. Forth, M. Gauns, R. N. Glud, M. M. M. Kuypers, G. Lavik, J. Milucka, S. W. A. Naqvi, A. Pratihary, N. P. Revsbech, B. Thamdrup, A. H. Treusch, and D. E. Canfield. N2 production in the Bay of Bengal Oxygen Minimum Zone. Unpubl.

Chipman, L., and others. 2012. Oxygen optodes as fast sensors for eddy correlation measurements in aquatic systems. Limnol. Oceanogr. Methods **10**: 304–316. doi:10.4319/lom.2012.10.304

Dalsgaard, T., B. Thamdrup, L. Farías, and N. P. Revsbech. 2012. Anammox and denitrification in the oxygen minimum zone of the eastern South Pacific. Limnol. Oceanogr. **57**: 1331–1346. doi:10.4319/lo.2012.57.5.1331

Delauney, L., C. Compère, and M. Lehaitre. 2010. Biofouling protection for marine environmental sensors. Ocean Sci. **6**: 503–511. doi:10.5194/os-6-503-2010

Draxler, S., M. E. Lippitsch, I. Klimant, H. Kraus, and O. S. Wolfbeis. 1995. Effects of polymer matrixes on the time-resolved luminescence of a ruthenium complex quenched by oxygen. J. Phys. Chem. **99**: 3162–3167. doi:10.1021/j100010a029

Ganesh, S., L. A. Bristow, M. Larsen, N. Sarode, B. Thamdrup, and F. J. Stewart. 2015. Size-fraction partitioning of community gene transcription and nitrogen metabolism in a marine oxygen minimum zone. ISME J. **9**: 2682–2696.

Garcia, H. E., and L. I. Gordon. 1992. Oxygen solubility in seawater: Better fitting equations. Limnol. Oceanogr. **37**: 1307–1312. doi:10.4319/lo.1992.37.6.1307

Glud, R. N., N. B. Ramsing, J. K. Gundersen, and I. Klimant. 1996. Planar optrodes: A new tool for fine scale measurements of two-dimensional O-2 distribution in benthic communities. Mar. Ecol. Prog. Ser. **140**: 217–226. doi:10.3354/meps140217

Glud, R. N., and others. 1999. Adaptation, test and in situ measurements with O2 microopt(r)odes on benthic landers. Deep Sea Res. Part I Oceanogr Res Pap. **46**: 171–183. doi:10.1016/S0967-0637(98)00068-5

Grasshoff, K. 1983. Determination of oxygen, p. 61–72 *In* K. Grasshoff, M. Ehrhardt, and K. Kremling [eds.], Methods of seawater analysis. Verlag Chemie GmbH.

Holst, G. A., M. Kuehl, and I. Klimant. 1995. Novel measuring system for oxygen micro-optodes based on a phase modulation technique, p. 387–98. European symposium on optics for environmental and public safety. International Society for Optics and Photonics.

Holtappels, M., L. Tiano, T. Kalvelage, G. Lavik, N. P. Revsbech, and M. M. M. Kuypers. 2014. Aquatic respiration rate measurements at low oxygen concentrations. PLoS ONE **9**: e89369. doi:10.1371/journal.pone.0089369

Kalvelage, T., and others. 2011. Oxygen sensitivity of Anammox and coupled N-cycle processes in oxygen minimum zones. PLoS ONE **6**: e29299. doi:10.1371/journal.-pone.0029299 doi:10.1371/journal.pone.0029299

Kautsky, H. 1939. Quenching of luminescence by oxygen. Trans Faraday Soc. **35**: 216–219. doi:10.1039/tf9393500216

Kirf, M., C. Dinkel, C. Schubert, and B. Wehrli. 2014a. Submicromolar oxygen profiles at the oxic–anoxic boundary of temperate lakes. Aquat. Geochem. **20**: 39–57. doi:10.1007/s10498-013-9206-7

Kirf, M. K., H. Røy, M. Holtappels, J. P. Fischer, C. J. Schubert, and B. Wehrli. 2014b. Redox gradients at the low oxygen boundary of lakes. Aquat. Sci. **77**: 81–93. doi:10.1007/s00027-014-0365-4

Klimant, I., V. Meyer, and M. Kuhl. 1995. Fiber-optic oxygen microsensors, a new tool in aquatic biology. Limnol. Oceanogr. **40**: 1159–1165. doi:10.4319/lo.1995.40.6.1159

Koren, K., L. Hutter, B. Enko, A. Pein, S. M. Borisov, and I. Klimant. 2013. Tuning the dynamic range and sensitivity of optical oxygen-sensors by employing differently substituted polystyrene-derivatives. Sens. Actuators B Chem. **176**: 344–350. doi:10.1016/j.snb.2012.09.057

Larsen, M., S. M. Borisov, B. Grunwald, I. Klimant, and R. N. Glud. 2011. A simple and inexpensive high resolution color ratiometric planar optode imaging approach: Application to oxygen and pH sensing. Limnol. Oceanogr. Methods **9**: 348–360. doi:10.4319/lom.2011.9.348

Lee, S. K., and I. Okura. 1997. Photostable optical oxygen sensing material: Platinum Tetrakis(pentafluorophenyl)-porphyrin immobilized in polystyrene. Anal. Commun. **34**: 185–188. doi:10.1039/a701130j

Lehner, P., C. Staudinger, S. M. Borisov, and I. Klimant. 2014. Ultra-sensitive optical oxygen sensors for characterization of nearly anoxic systems. Nat. Commun. **5**:4460. doi:10.1038/ncomms5460

Lehner, P., and others. 2015. LUMOS—a sensitive and reliable optode system for measuring dissolved oxygen in the nanomolar range. PLoS ONE **10**: e0128125. doi:10.1371/journal.pone.0128125

Li, Y., and others. 2010. Direct functionalization of polycyclic aromatics via radical perfluoroalkylation. Organ. Lett. **12**: 2374–2347. doi:10.1021/ol1007197

Martini, M., B. Butman, and M. J. Mickelson. 2007. Long-term performance of Aanderaa optodes and sea-bird SBE-43 dissolved-oxygen sensors bottom mounted at 32 m in Massachusetts Bay. J. Atmos. Oceanic Technol. **24**: 1924–1935. doi:10.1175/JTECH2078.1

Mcneil, C. L., and E. A. D'asaro. 2014. A calibration equation for oxygen optodes based on physical properties of the sensing foil. Limnol. Oceanogr. Methods **12**: 139–154. doi:10.4319/lom.2014.12.139

Navarro-Villoslada, F., and others. 2001. Fiber-optic luminescent sensors with composite oxygen-sensitive layers and anti-biofouling coatings. Anal. Chem. **73**: 5150–5016. doi:10.1021/ac015517n [10.1021/ac015517n]

Nestler, H., B. Kiesel, S. Kaschabek, M. Mau, M. Schlömann, and G. Balcke. 2007. Biodegradation of chlorobenzene under hypoxic and mixed hypoxic-denitrifying conditions. Biodegradation **18**: 755–767. doi:10.1007/s10532-007-9104-z

Oguri, K., H. Kitazato, and R. N. Glud. 2006. Platinum octaetylporphyrin based planar optodes combined with an UV-LED excitation light source: An ideal tool for high-resolution O2 imaging in O2 depleted environments. Mar. Chem. **100**: 95–107. doi:10.1016/j.marchem.2005.11.005

Quaranta, M., S. Borisov, and I. Klimant. 2012. Indicators for optical oxygen sensors. Bioanal. Rev. **4**: 115–157. doi:10.1007/s12566-012-0032-y

Revsbech, N. P. 1989. An oxygen microsensor with a guard cathode. Limnol. Oceanogr. **34**: 474–478. doi:10.4319/lo.1989.34.2.0474

Revsbech, N. P., L. H. Larsen, J. Gundersen, T. Dalsgaard, O. Ulloa, and B. Thamdrup. 2009. Determination of ultra-low oxygen concentrations in oxygen minimum zones by the STOX sensor. Limnol. Oceanogr. Methods **7**: 371–381. doi:10.4319/lom.2009.7.371

Revsbech, N. P., B. Thamdrup, T. Dalsgaard, and D. E. Canfield. 2011. Chapter fourteen—construction of STOX oxygen sensors and their application for determination of O2 concentrations in oxygen minimum zones, p. 325–341. *In* G. K. Martin [ed.], Methods in enzymology. Academic Press.

Rickelt, L. F., L. Askaer, E. Walpersdorf, B. Elberling, R. N. Glud, and M. Kuhi. 2013. An optode sensor array for long-term in situ oxygen measurements in soil and sediment. J. Environ. Qual. **42**: 1267–1273. doi:10.2134/jeq2012.0334

Santner, J., M. Larsen, A. Kreuzeder, and R. N. Glud. 2015. Two decades of chemical imaging of solutes in sediments and soils—a review. Anal. Chim. Acta **878**: 9–42. doi:10.1016/j.aca.2015.02.006

Schmälzlin, E., and others. 2005. An optical multifrequency phase-modulation method using microbeads for measuring intracellular oxygen concentrations in plants. Biophys. J. **89**: 1339–1345. doi:10.1529/biophysj.105.063453

Schutting, S., I. Klimant, D. De Beer, and S. Borisov. M. 2014. New highly fluorescent pH indicator for ratiometric RGB imaging of pCO 2. Methods Appl. Fluoresc. **2**: 024001. doi:10.1088/2050-6120/2/2/024001

Stich, M. I. J., S. M. Borisov, U. Henne, and M. Schäferling. 2009. Read-out of multiple optical chemical sensors by means of digital color cameras. Sens. Actuators B Chem. **139**: 204–207. doi:10.1016/j.snb.2008.12.036

Stolper, D. A., N. P. Revsbech, and D. E. Canfield. 2010. Aerobic growth at nanomolar oxygen concentrations. Proc Natl Acad Sci. USA **107**: 18755–18760. doi:10.1073/pnas.1013435107

Tengberg, A., and others. 2006. Evaluation of a lifetime-based optode to measure oxygen in aquatic systems. Limnol. Oceanogr. Methods **4**: 7–17. doi:10.4319/lom.2006.4.7

Thamdrup, B., T. Dalsgaard, and N. P. Revsbech. 2012. Widespread functional anoxia in the oxygen minimum zone of the Eastern South Pacific. Deep Sea Res. Part I Oceanogr Res Pap. **65**: 36–45. doi:10.1016/j.dsr.2012.03.001

Tiano, L., and others. 2014. Oxygen distribution and aerobic respiration in the north and south eastern tropical Pacific oxygen minimum zones. Deep Sea Res. Part I Oceanogr. Res. Pap. **94**: 173–183. doi:10.1016/j.dsr.2014.10.001

Uchida, H., T. Kawano, I. Kaneko, and M. Fukasawa. 2008. In situ calibration of optode-based oxygen sensors. J. Atmos. Oceanic Technol. **25**: 2271–2281. doi:10.1175/2008JTECHO549.1

Ulloa, O., D. E. Canfield, E. F. Delong, R. M. Letelier, and F. J. Stewart. 2012. Microbial oceanography of anoxic oxygen minimum zones. Proc Natl Acad. Sci. USA **109**: 15996–6003. doi:10.1073/pnas.1205009109

Wang, X. D., and O. S. Wolfbeis. 2014. Optical methods for sensing and imaging oxygen: Materials, spectroscopies and applications. Chem. Soc. Rev. **43**: 3666–3761. doi:10.1039/c4cs00039k

Wencel, D., J. Moore, N. Stevenson, and C. Mcdonagh. 2010. Ratiometric fluorescence-based dissolved carbon dioxide sensor for use in environmental monitoring

applications. Anal. Bioanal. Chem. **398**: 1899–1907. doi: 10.1007/s00216-010-4165-y

Winkler, L. W. 1888. Die Bestimmung des im Wasser gelösten Sauerstoffes. Berichte Der Deutschen Chemischen Gesellschaft. **21**: 2843–2854. doi:10.1002/cber.188802102122

Acknowledgments

We are grateful for the skillful help from Per Martensen, Torben Christensen, and Klaus L. Petersen, from the mechanical workshop at SDU. Anni Glud is thanked for construction of the STOX sensors for the ETNP cruise. Preben G. Sørensen for constructing the STOX sensors for the BoB cruise. Henrik Larsen is thanked for fruitful discussions and guidance in the design stage of the instrument electronics. Laura A. Bristow is thanked for processing CTD data and help during the cruises and field-testing the Mini-TOP.

The work was financially supported by: ERC Advanced Grant, ERC-2010-AdG_20100224, Grant Agreement Number 267233, OXYGEN; ERC Advanced Grant, ERC-AdG-2014_669947_HADES; The Danish National Research Foundation (#DNRF53 to Nordic Center for Earth Evolution); The Commission for Scientific Research in Greenland (KVUG; GCRC6507), The Danish Council for Independent Research (12-125843; 0602-02276B), and the Villum Foundation; The US National Science Foundation, grant 1151698. We thank two anonymous reviewers for their constructive criticism that helped improve the manuscript.

Submitted 4 March 2016
Revised 16 June 2016
Accepted 19 June 2016

Associate editor: Mike DeGrandpre